Published in final edited form as:
Int J Radiat Oncol Biol Phys. 2009 October 1; 75(2): . doi:10.1016/j.ijrobp.2009.06.007.

A Novel Murine Model for Localized Radiation Necrosis and its Characterization using Advanced Magnetic Resonance Imaging

Sarah C. Jost, M.D.[#], **Andrew Hope, M.D.**[†], **Erich Kiehl, B.S.**, **Arie Perry, M.D.**, **Sarah Travers**, and **Joel R. Garbow, Ph.D.**[*]
Departments of Neurosurgery (SCJ), Radiation Oncology (AH, EK), Pathology and Immunology (AP), and Radiology (ST, JRG) and The Alvin J. Siteman Cancer Center (JRG), Washington University School of Medicine, St. Louis, MO 63110

Abstract

Introduction—Magnetic resonance (MR) images following external beam radiotherapy for brain tumors often display signal changes characteristic of either tumor progression and/or radiation injury. No non-invasive diagnostic biomarkers have been identified that clearly distinguish between these two disease processes. This study's objective was to develop a murine model of radiation necrosis using fractionated, sub-total cranial irradiation and to investigate the imaging signature of radiation-induced tissue damage using advanced MR imaging techniques.

Methods—Twenty four mice each received 60 Gy of hemispheric (left) irradiation in ten equal fractions. MR images at 4.7 T were subsequently collected using T1-, T2- and diffusion-sequences at selected time points following irradiation or implantation. Following imaging, animals were euthanized and their brains were fixed for correlative histology.

Results—Contrast-enhanced T1- and T2-weighted MR images at months 2, 3, and 4 showed changes consistent with progressive radiation necrosis. Quantitatively, mean diffusivity was significantly higher (mean = 0.86, 1.13, and 1.24 $\mu m^2/ms$ at 2, 3, and 4 months, respectively) in radiated brain, compared with contralateral untreated brain tissue (mean = 0.78, 0.82, and 0.83 $\mu m^2/ms$) ($p<0.0001$). Histology reflected changes typically seen in radiation necrosis.

Conclusions—This murine model of radiation necrosis will facilitate investigation of imaging biomarkers that distinguish between radiation necrosis and tumor recurrence. In addition, this preclinical study supports clinical data suggesting that DWI may be helpful in answering this diagnostic question in clinical settings.

Keywords

Radiation necrosis; Conformal radiation; Animal models; Magnetic Resonance Imaging; Brain tumor

[*]Corresponding author: Joel R. Garbow, Ph.D., Department of Radiology, Washington University School of Medicine, Campus Box 8227, 4525 Scott Avenue, St. Louis, MO 63110, garbow@wustl.edu, Phone: 314 362 9949, Fax: 314 362 0526.
[#]Current Address: Swedish Neuroscience Institute, Center for Advanced Brain Tumor Treatment Swedish Hospital Seattle, WA 98122
[†]Current Address: 610 University Ave, Princess Margaret Hospital, Toronto, Ontario, M5G 2M9 Canada

Conflict of Interest
None of the authors of this manuscript have a conflict of interest to declare.

Introduction

The management of malignant brain tumors remains a challenging clinical problem. Patients with such tumors typically receive multimodal therapy, including surgical resection, chemotherapy, and radiation. Over the past decade, patient outcomes have benefitted from numerous advances, including novel chemotherapeutic agents, improved surgical resection (including the use of surgical navigation systems and intra-operative imaging), conformal radiation therapy, and more biologically relevant imaging modalities. Nonetheless, in malignant primary brain tumors, patient outcomes remain poor. Patients with glioblastoma, the most common primary malignant neoplasm of the adult brain {Davis FG, 1998 #11; Tooth HH, 1912 #17}, have a median survival of only 12 to 15 months with 2-year survival rates of less than 30% {Prados M, 2000 #15; Stupp R, 2005 #20}.

Patients with malignant brain tumors are typically treated with a combination of surgical resection, chemotherapy, and external-beam radiotherapy. As no combination of treatments has yet proven curative, the majority of patients eventually experience a recurrence of their tumor. A significant subset of patients who undergo a combination of surgery, chemotherapy and radiation develop MR imaging findings following these therapies that are often difficult to interpret. Radiation necrosis is the most common and most significant of these treatment-associated changes and it is particularly challenging because its anatomic imaging characteristics are remarkably similar to those of recurrent tumor. For patients whose post-radiation MR scans show contrast enhancement and T2-weighted image hyperintensity, the clinical diagnosis is typically ‘recurrence *vs*. radiation necrosis’. Distinguishing between these two clinical different entities is a significant challenge for treating physicians.

The development of non-invasive imaging markers of diagnostic specificity is an important goal for clinicians caring for patients with brain tumors. Recent advances in imaging, specifically exploiting PET imaging tracers that measure cell proliferation {Jost SC, 2007 #32; Spaeth N, 2004 #24; Spaeth, 2006 #40} and advanced MR imaging techniques, including perfusion and diffusion-weighted imaging (DWI), afford unique opportunities to monitor tumor biology *in vivo*. Although researchers have suggested that advanced imaging modalities more readily distinguish radiation necrosis from recurrent tumor {Hein PA, 2004 #8; Schlemmer HP, 2002 #5; Weybright P, 2005 #4; Zeng QS, 2007 #6}, no single imaging modality with sufficient diagnostic sensitivity and specificity has yet been identified.

Diffusion-weighted MR imaging (DWI) provides a method for the *in vivo* measurement of the diffusivity of water in tissue. Diffusion imaging is sensitive to the microstructure of biological tissue on a distance scale of 1–10 microns and, as such, may reflect changes in tumor-cell density. Water diffusion in tissues is restricted by interactions with organelles, cell membranes, and other cellular barriers. Ross and colleagues have demonstrated that malignant tumors have a high cellular density and corresponding low diffusivity, and that changes in ADC correlate with tumor response to cytotoxic therapy in malignant gliomas, both in rat models {Chenevert TL, 1997 #9; Chenevert TL, 2000 #10; Hall DE, 2004 #12} and in humans {Moffat BA, 2005 #13; Moffat BA, 2006 #14}. In clinical research studies, both MR spectroscopy and DWI have also been used to distinguish recurrent glioma from radiation necrosis {Hein PA, 2004 #8; Schlemmer HP, 2002 #5; Weybright P, 2005 #4; Zeng QS, 2007 #6}. In these preliminary studies, the apparent diffusion coefficient (ADC) change following radiation was higher than that due to recurrent tumor. However, these studies, in isolation, lack the sensitivity and specificity to unambiguously distinguish necrosis from tumor and have often been limited by inadequate statistical power and a lack of histological correlation.

Until recently, few small-animal models of radiation necrosis in brain tissue have been reported {Ernst-Stecken A, 2007 #27; Ishikawa S, 1999 #28; Rabinov JD, 2006 #30; Sun X, 2004 #31}. Previous models were developed primarily in rats and employed only a small number of radiation fractions. Herein we describe the development of a radiation necrosis model in mice that employs focal, multi-fraction radiation to more accurately reflect the clinical situation encountered by patients treated for malignant brain tumors.

The recent development of a conformal pre-clinical irradiation system {Kiehl EL, 2008 #21} demonstrated that high dose, focal, fractionated brain irradiation in small animals is feasible and can generate relevant pre-clinical models of brain tumors {Goldhoff P, 2008 #37}. We hypothesized that this new technology could be used to create a murine model of radiation necrosis, using hemispheric irradiation in a dose and fractionation scheme patterned after therapeutic doses of radiation used to treat human patients with glioma. We also hypothesized that longitudinal small-animal imaging and, in particular, diffusion-weighted MRI, may demonstrate a distinctive imaging signature for radiation necrosis, relative to signals seen normal brain tissue.

Building upon our experience in conformal irradiation {Kiehl EL, 2008 #21; Goldhoff P, 2008 #37} and MR imaging of murine models of brain tumors {Banerjee, 2007 #33; Jost SC, 2007 #32}, the goals of this work were to develop a murine model of radiation necrosis, to characterize the imaging signature of radiation-induced tissue damage using DWI, and to compare these imaging characteristics with the signals seen in un-irradiated brain.

Materials Methods

Small Animal Models

All studies were performed in accordance with the guidelines of the Washington University Animal Studies Committee (ASC) and in accordance with protocols approved by the Washington University Division of Comparative Medicine that met or exceeded American Association for the Accreditation of Laboratory Animal Care standards. A total of thirty-two subject animals were included in this study. Twenty-four female Balb/c mice were irradiated with a total of 60 Gy of radiation (10 × 6 Gy), as described below, and the resulting brain parenchymal changes were characterized by both MRI and histology. Mice were 12–16 weeks old upon initiation of either radiation therapy. All animals were observed daily and weighed twice weekly to ensure that interventions were well tolerated.

Small-Animal Irradiation

The components of the microRT system have been described previously {Kiehl EL, 2008 #21; Stojadinovic S, 2007 #23; Stojadinovic S, 2006 #22}. For the hemispheric irradiation, all animals were treated with one vertex beam at the 0° microRT treatment position, prescribed to midline, for a total of 6 Gy per fraction per animal, dosed daily Monday through Friday for two weeks. The animals were treated according to the generated radiotherapy plans using a clinical Ir-192 HDR remote after-loading system (Nucletron; Columbia, Maryland) collimated *via* the microRT collimator system. Given the inputted couch coordinates and the targeted fraction dose, treatment times were calculated using the modified parametric beam and dose models described previously {Stojadinovic S, 2007 #23; Stojadinovic S, 2006 #22}.

Small Animal Imaging

Mice treated with fractionated radiation were observed clinically, weighed twice weekly, and followed for two months to ensure that they did not exhibit systemic symptoms of radiation toxicity. Initiation of *in vivo* small-animal imaging was deferred in these animals

until two months after radiation because previous studies at lower dose and longer fractionation schemes had shown no MR-detectable radiation-induced brain injury at up to ten months post radiation therapy (data not shown). Cohorts of eight animals were imaged at two, three and four months following the completion of fractionated irradiation.

Anatomic MRI

Images were collected in an Oxford Instruments 4.7-T magnet (33 cm, clear bore) equipped with 15-cm inner diameter, actively shielded gradient coils (maximum gradient, 18 G/cm; rise time ~ 200 μs). The magnet/gradients are interfaced with a Varian (Palo Alto, CA) INOVA console, and data were collected using a 1.5-cm OD surface coil (receive) and a 9-cm ID Helmholtz coil (transmit). Before the imaging experiments, mice were anesthetized with isoflurane/O_2 [3% (v/v)], and maintained on isoflurane/O_2 [1.25% (v/v)] throughout the experiments.

Mice were injected intraperitoneally with 500 μl Omniscan (Gadodiamide, GE Healthcare) contrast agent, diluted 1:10 in sterile saline, 15 minutes prior to being placed in the magnet. T1-weighted, gradient-echo multi-slice transaxial images were collected (TR = .125 s, TE = .0025 s, FOV = 1.5 × 1.5 cm^2, slice thickness = 0.5 mm). In addition, T2-weighted, multi-slice spin-echo coronal images were collected for each animal (TR = 1.5 s; TE = .05 s; FOV = 1.5 × 1.5 cm^2; thickness = 0.5 mm). Regions of interest were identified *post hoc* with the public domain program ImageJ, available at http://rsb.info.nih.gov/imagej.

Diffusion-Weighted Imaging

Diffusion-weighted MR images were collected using a standard spin-echo pulse sequence with the addition of diffusion-sensitizing gradients with multiple b values ranging from 0 to 2300 s/mm^2. Diffusion imaging parameters include: TR = 1.5 s, TE = 0.05 s, time between diffusion gradient pulses (Δ) = 25 ms, diffusion gradient duration (δ) = 10 ms, and signal averages (NEX) = 8.

DWI processing and data analysis

Diffusion data were modeled on a pixel-by-pixel basis as a monoexponential decay using Bayesian Probability Theory (BPT) software developed in our laboratory {Bretthorst, 2005 #34; Bretthorst, 2005 #35}. For each pixel, intensity *vs.* b-value data were fit with a single exponential function decaying to a non-zero constant, from which maps of apparent diffusion coefficient (ADC) were derived. Data analysis was performed on a slice-by-slice basis by placing regions of interest (ROIs) around areas of anomalous, hyperintense signal on b=0 (non-diffusion weighted, T2-weighted, spin-echo) images. ROIs of similar size and shape were also placed in the contralateral hemisphere in each slice. ROIs selected on the anatomic images were saved and then overlaid onto the corresponding ADC maps, and ADC data for each voxel within each ROI were extracted.

Histology

Irradiated mice whose MR images were suggestive of radiation necrosis were euthanized for histological analysis at two (4 mice), three (4 mice) and four (6 mice) months post-irradiation, immediately following imaging. A total of fourteen animals were euthanized and their brains were formalin fixed and stained with H&E using standard protocols.

Statistical Analysis

For each animal, ADC values for all selected ROIs (irradiated and contralateral) were calculated. The mean, median, variance and standard deviation were calculated on a per animal basis at each time point. Mean ADC values were then compared across time points

and between tissue types using the student's t-test. The raw data from each of these analyses were also compiled into box-and-whisker plots so that the range and variance of the data could be readily displayed.

Results

A total of 24 mice were irradiated with 60 Gy of irradiation each, fractionated over 2 weeks, followed by serial MR imaging. The radiation plan is shown in Figure 1 as a color map overlaid onto a representative MR image of mouse brain. It is clear from this plan that the irradiation is limited effectively to the left hemisphere of the brain, with the highest dose delivered at the brain's surface. Three cohorts of eight mice each were imaged at 2, 3, and 4 months following completion of hemispheric irradiation. After the completion of each month's MR experiments, a subset of these mice was euthanized for histological analysis. Both contrast-enhanced gradient-echo and spin-echo sequences showed changes consistent with tissue damage and breakdown of the blood-brain barrier. Figure 2 shows this contrast enhancement and T2-weighted image hyper-intensity, with progressive signal and heterogeneity, for representative animals at 2, 3, and 4 months post irradiation.

Mice consistently showed left hemispheric anatomic signal changes consistent with those seen in human patients with post-treatment radiation necrosis. Histology also reflected changes typically observed in radiation necrosis (Figure 3), with fibrinoid vascular necrosis, coagulative parenchymal necrosis with macrophage infiltration, and vascular telangiectasia seen increasingly over the three-month time course of the study. Other features included cerebral edema, tissue rarefaction with decreased cellularity, and reactive astrocytosis.

Significant changes in diffusion signal were also seen in the left hemisphere of irradiated mice. Figure 4 shows ADC maps for representative mice at 2, 3, and 4 months post irradiation. Qualitatively, one can identify asymmetry and increased diffusivity in the left hemisphere, particularly in the third and fourth months following irradiation. From our ROI analysis, mean diffusivity was significantly higher (mean = 0.86, 1.13, and 1.24 μm^2/ms at 2, 3, and 4 months) in radiated brain, compared with contralateral, untreated brain tissue (mean = 0.78, 0.82, and 0.83 μm^2/ms) ($p<0.0001$). The mean, median, and range of diffusion data from all voxels in regions of interest in each radiated animal are shown graphically in box-and-whisker plots in Figure 5. Note that if small ROIs are drawn around the most hyperintense regions in the anatomic images of the irradiated hemisphere, mean diffusivities at 3 and 4 months postirradiation are approximately 10% higher than the values reported above. These data clearly demonstrate the time progression of the diffusion signal following irradiation and allow direct comparison with data for brain tissue in the untreated, contralateral hemisphere.

Discussion

Serial/longitudinal MR imaging in small-animal models of tumor and/or radiation necrosis provides a significant opportunity to investigate novel imaging methods for distinguishing radiation necrosis from growing tumor, with imaging findings directly supported by correlative histology. This allows positive results to be readily translated to clinical research investigations. Small-animal models of brain tumors have been extensively reported in the literature {Fomchenko, 2006 #36}. These models cover a wide range of paradigms for tumor development, including direct implantation of orthotopic tumor cell lines {Jost SC, 2007 #32}, genetic models of spontaneous tumor development {McConville P, 2007 #38}, implantation of human tumor cell lines (such as the U87 cell line) into nude mice {Goldhoff P, 2008 #37; Kiehl EL, 2008 #21}, and generation of tumors from stem cell lines.

Characterization of the imaging signature using advanced imaging biomarkers is ongoing in our laboratory and other laboratories worldwide.

The lack of animal models for radiation necrosis has significantly limited the development of methods for distinguishing necrosis from tumor re-growth. Until recently, irradiation of small animals, particularly mice, was performed by irradiating a large portion of the animal's body rather than directing radiation doses to focal targets. Prior pre-clinical brain irradiations have been predominated by non-targeted dose delivery produced by single, high dose, full-body radiation fields with selective shielding to allow whole brain irradiation {Akiyama K, 2001 #26; Mizumatsu S, 2003 #2; Monje ML, 2003 #1; Panagiotakos G, 2007 #29; Yuan H, 2007 #3}. Without shielding, the normal tissue effects of radiation limit the dose of radiation that can be given to a small animal. Even with shielding, traditional approaches limit the ability to specifically target a small focal region of the brain. Researchers have, however, shown histological evidence of tissue damage with whole brain irradiation. More recently, the advance of stereotactic radiosurgery (SRS) has prompted researchers to consider SRS as a method for inducing damage to normal tissue {Jirak, 2007 #39}. Studies have separately considered both the imaging and histological characteristics of focal tissue damage in this setting {Ishikawa S, 1999 #28; Jirak, 2007 #39; Rabinov JD, 2006 #30} as well as in select hypofractionated settings {Ernst-Stecken A, 2007 #27; Sun X, 2004 #31}.

To date, however, investigations have not thoroughly characterized tissue changes resulting from focal fractionated radiation at clinically relevant doses with advanced small-animal imaging methods such as diffusion, perfusion, molecular imaging, or spectroscopy. Combining conformal irradiation of a single hemisphere of the brain with advanced MR sequences and correlative histology creates a system well-suited for prospective studies comparing the tissue effects of fractionated radiation with small animal models of tumor growth. This study demonstrates a novel, mouse model of radiation necrosis, characterized with anatomic MR imaging, DWI, and histology.

To consistently induce radiation necrosis and simplify the model, an aggressive radiation dose fractionation (6 Gy × 10) and schedule (2 weeks) were selected. While the resulting dose is substantially higher than a clinical-dose schedule, this schedule was chosen because Phase I studies of dose escalation have consistently shown a relatively low risk of radiation necrosis, even with high doses of conventionally fractionated radiation (66–84 Gy) {Tsien, 2009 #41}. The resulting radiation necrosis was histologically similar to that induced in patients (Figure 3), suggesting that this model of necrosis may be translatable.

Administration of 60 Gy of fractionated hemispheric conformal irradiation reliably induces damage to the brain parenchyma which is progressive, visible on MR imaging, and shows histologically the classic tissue changes associated with radiation necrosis, including tissue edema, necrosis, decreased cellularity, extravasation of blood around telangiectatic blood vessels, and fibrinoid vascular necrosis. Anatomic MR images show signal changes within radiated tissue that are similar to those seen in growing tumors (e.g., uptake of gadolinium contrast and T2-weighted image hyperintensity).

Previous human studies have failed to identify an imaging paradigm with the sensitivity and specificity to consistently distinguish between recurrent tumor and radiation necrosis. The heterogeneity of different tumor types, the co-existence of tumor within the setting of radiation change, and the lack of confirmatory histology combine to create confounding factors that make these human studies particularly challenging. This small-animal model of radiation necrosis will provide a platform for the development of non-invasive imaging methods for distinguishing radiation change from growing tumor. Particularly challenging is

the characterization of brain that contains both regions of radiation necrosis and tumors as is often the case in glioma patients biopsied post-therapy. Our murine model of necrosis provides an excellent paradigm for probing this heterogeneous condition, which can be created by orthotopic implantation of tumor cells into radiation-induced necrotic tissue. While data in this work were analyzed on a region-of-interest basis, MRI's high resolution allows pixel-by-pixel analysis of images and parametric ADC maps to be performed. Such analysis is a key to the detailed correlation of imaging data, radiation dose, and histology needed to develop a robust strategy for distinguishing necrosis and tumor. Experiments to probe heterogeneous, 'mixed-case' tumor/necrosis conditions in animals and to develop pixel-by-pixel analysis strategies are ongoing in our laboratory. It is anticipated that, once properly validated, this imaging methodology will translate readily to humans, providing an important tool in the diagnosis and treatment of brain-tumor patients.

Acknowledgments

We thank Drs. Joseph J. H. Ackerman, Joshua Rubin, Daniel A. Low, and Enrique Izaguirre for helpful discussions and Dr. Neha Dahiya for assistance in reviewing the mouse histology. This work was supported by an NIH/NCI Small Animal Imaging Resource Program (SAIRP) grant (U24 CA83060), an NIH grant supporting development of microRT (R21 CA108677), the Alvin J. Siteman Cancer Center at Washington University in St. Louis, an NCI Comprehensive Cancer Center (P30 CA91842), and the Saint Louis Brain Tumor Foundation.

References

1. Davis FG, Freels S, Grutsch J, et al. Survival rates in patients with primary malignant brain tumors stratified by patient age and tumor histological type: an analysis based on Surveillance, Epidemiology, and End Results (SEER) data, 1973–1991. J Neurosurg. 1998; 88:1–10. [PubMed: 9420066]
2. Tooth HH. Some observations on the growth and survival period of intracranial tumours, based on the records of 500 cases. Brain. 1912; 35:61–108.
3. Prados M, Levin V. Biology and treatment of malignant glioma. Semin Oncol. 2000; 27:1–10. [PubMed: 10866344]
4. Stupp R, Mason WP, van den Bent MJ, et al. Radiotherapy plus concomitant and adjuvant temozolomide for glioblastoma. N Engl J Med. 2005; 352:987–996. [PubMed: 15758009]
5. Jost SC, Wanebo JE, Song SK, et al. Small Animal Imaging as a Tool for In Vivo Monitoring in a Murine Model for Glioblastoma. Neurosurgery. 2007; 60:360–370. [PubMed: 17290188]
6. Spaeth N, Wyss MT, Weber B, et al. Uptake of 18F-fluorocholine, 18F-fluoroethyl-L-tyrosine, and 18F-FDG in acute cerebral radiation injury in the rat: implications for separation of radiation necrosis from tumor recurrence. J Nucl Med. 2004; 45:1931–1938. [PubMed: 15534065]
7. Spaeth N, Wyss MT, Pahnke J, et al. Uptake of 18F-fluorocholine, 18F-fluoro-ethyl-L: -tyrosine and 18F-fluoro-2-deoxyglucose in F98 gliomas in the rat. Eur J Nucl Med Mol Imaging. 2006; 33:673–682. [PubMed: 16538503]
8. Hein PA, Esley CJ, Dunn JF, et al. Diffusion-weighted imaging in the follow-up of treated high-grade gliomas: tumor recurrence versus radiation injury. Am J Neuroradiology. 2004; 25:201–209.
9. Schlemmer HP, Bachert P, Henze M, et al. Differentiation of radiation necrosis from tumor progression using proton magnetic resonance spectroscopy. Neuroradiology. 2002; 44:216–222. [PubMed: 11942375]
10. Weybright P, Sundgren PC, Maly P, et al. Differentiation between brain tumor recurrence and radiation injury using MR spectroscopy. Am J Roentgenol. 2005; 185:1471–1476. [PubMed: 16304000]
11. Zeng QS, Li CF, Liu H, et al. Distinction between recurrent glioma and radiation injury using magnetic resonance spectroscopy in combination with diffusion weighted imaging. Int J Radiation Oncology Biol Phys. 2007; 68:151–158.
12. Chenevert TL, McKeever PE, Ross BD. Monitoring Early Response of Experimental Brain Tumors to Therapy Using Diffusion Magnetic Resonance Imaging. Clin Cancer Res. 1997; 3:1457–1466. [PubMed: 9815831]

13. Chenevert TL, Stegman LD, Taylor JM, et al. Diffusion Magnetic Resonance Imaging: Early Surrogate Marker of Therapeutic Efficacy in Brain Tumors. J Natl Cancer Inst. 2000; 92:2029–2036. [PubMed: 11121466]
14. Hall DE, Moffat BA, Stojanovska J, et al. Therapeutic efficacy of DTI-015 using diffusion magnetic resonance imaging as an early surrogate marker. Clin Cancer Res. 2004; 10:7852–7859. [PubMed: 15585617]
15. Moffat BA, Chenevert TL, Lawrence TS, et al. Functional diffusion map: A noninvasive MRI biomarker for stratification of clinical brain tumor response. Proc Natl Acad Sci USA. 2005; 102:5524–5529. [PubMed: 15805192]
16. Moffat BA, Chenevert TL, Meyer CR, et al. The Functional Diffusion Map: An Imaging Biomarker for the Early Prediction of Cancer Treatment Outcome. Neoplasia. 2006; 8:259–267. [PubMed: 16756718]
17. Ernst-Stecken A, Jeske I, Hess A, et al. Hypofractionated stereotactic radiotherapy to the rat hippocampus. Determination of dose response and tolerance. Strahlenther Onkol. 2007; 183:440–446. [PubMed: 17680224]
18. Ishikawa S, Otsuki T, Kaneki M, et al. Dose-related effects of single focal irradiation in the medial temporal lobe structures in rats--magnetic resonance imaging and histological study. Neurol Med Chir (Tokyo). 1999; 39:1–7. [PubMed: 10093454]
19. Rabinov JD, Cheng LL, Lee PL, et al. MR spectroscopic changes in the rat hippocampus following proton radiosurgery. Stereotact Funct Neurosurg. 2006; 84:147–154. [PubMed: 16899979]
20. Sun X, Takahashi S, Kubota Y, et al. Experimental model for irradiating a restricted region of the rat brain using heavy-ion beams. J Med Invest. 2004; 51:103–107. [PubMed: 15000263]
21. Kiehl EL, Stojadinovic S, Malinowski KT, et al. Feasibility of small animal cranial irradiation with the microRT system. Med Phys. 2008; 35:4735–4743. [PubMed: 18975718]
22. Goldhoff P, Warrington N, Limbrick DD, et al. Targeted inhibition of phosphodiesterase type 4 promotes brain tumor regression. Clin Cancer Res. 2008 in press.
23. Banerjee D, Hegedus B, Gutmann DH, et al. Detection and measurement of neurofibromatosis-1 mouse optic glioma in vivo. Neuroimage. 2007; 35:1434–1437. [PubMed: 17383899]
24. Stojadinovic S, Low DA, Hope AJ, et al. MicroRT-small animal conformal irradiator. Med Phys. 2007; 34:4706–4716. [PubMed: 18196798]
25. Stojadinovic S, Low DA, Vicic M, et al. Progress toward a microradiation therapy small animal conformal irradiator. Med Phys. 2006; 33:3834–3845. [PubMed: 17089848]
26. Bretthorst GL, Hutton WC, Garbow JR, et al. Exponential Model Selection (In NMR) Using Bayesian Probability Theory. Concepts Magn Reson, Part A. 2005; 27A:64–72.
27. Bretthorst GL, Hutton WC, Garbow JR, et al. Exponential Parameter Estimation (In NMR) Using Bayesian Probability Theory. Concepts Magn Reson, Part A. 2005; 27A:55–63.
28. Fomchenko EI, Holland EC. Mouse models of brain tumors and their applications in preclinical trials. Clin Cancer Res. 2006; 12:5288–5297. [PubMed: 17000661]
29. McConville P, Hambardzumyan D, Moody JB, et al. Magnetic resonance imaging determination of tumor grade and early response to temozolomide in a genetically engineered mouse model of glioma. Clin Cancer Res. 2007; 13:2897–2904. [PubMed: 17504989]
30. Akiyama K, Tanaka R, Sato MT, et al. Cognitive dysfunction and histological findings in adult rats one year after whole brain irradiation. Neurol Med Chir (Tokyo). 2001; 41:590–598. [PubMed: 11803584]
31. Mizumatsu S, Monje ML, Morhardt DR, et al. Extreme sensitivity of adult neurogenesis to low doses of X-irradiation. Cancer Res. 2003; 63:4021–4027. [PubMed: 12874001]
32. Monje ML, Toda H, Palmer TD. Inflammatory blockade restores adult hippocampal neurogenesis. Science. 2003; 302:1760–1765. [PubMed: 14615545]
33. Panagiotakos G, Alshamy G, Chan B, et al. Long-Term Impact of Radiation on the Stem Cell and Oligodendrocyte Precursors in the Brain. PLoS ONE. 2007; 2:e588. [PubMed: 17622341]
34. Yuan H, Gaber MW, Boyd K, et al. Effects of fractionated radiation on the brain vasculature in a murine model: blood-brain barrier permeability, astrocyte proliferation, and ultrastructural changes. International Journal of Radiation Oncology and Biological Physics. 2007; 66:860–866.

35. Jirak D, Namestkova K, Herynek V, et al. Lesion evolution after gamma knife irradiation observed by magnetic resonance imaging. Int J Radiat Biol. 2007; 83:237–244. [PubMed: 17575951]

36. Tsien C, Moughan J, Michalski JM, et al. Phase I three-dimensional conformal radiation dose escalation study in newly diagnosed glioblastoma: Radiation Therapy Oncology Group Trial 98-03. Int J Radiat Oncol Biol Phys. 2009; 73:699–708. [PubMed: 18723297]

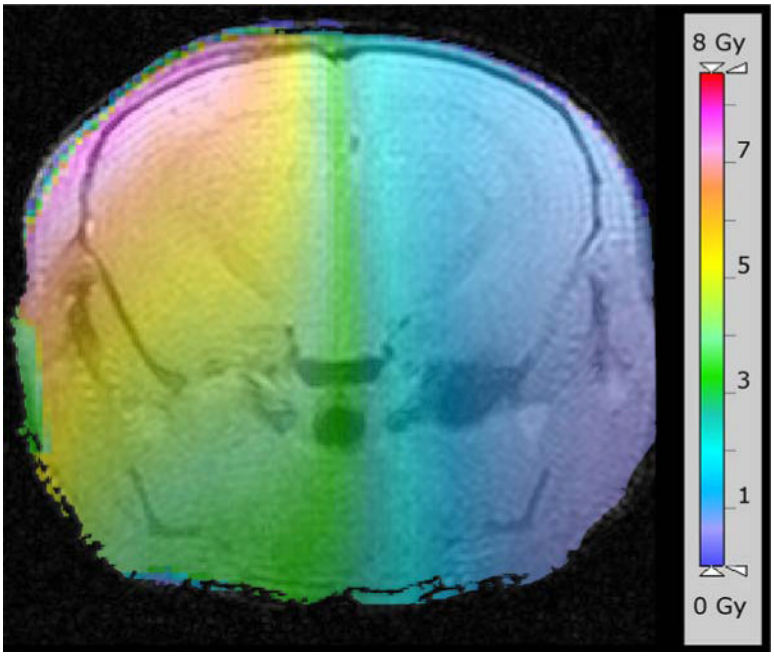

Figure 1.
Radiation plan, shown as a color map overlaid onto a representative MR image of mouse brain. The scale bar on the right indicates the radiation dose delivered to the brain. Irradiation is limited effectively to the left hemisphere of the brain, with the highest dose delivered at the brain's surface.

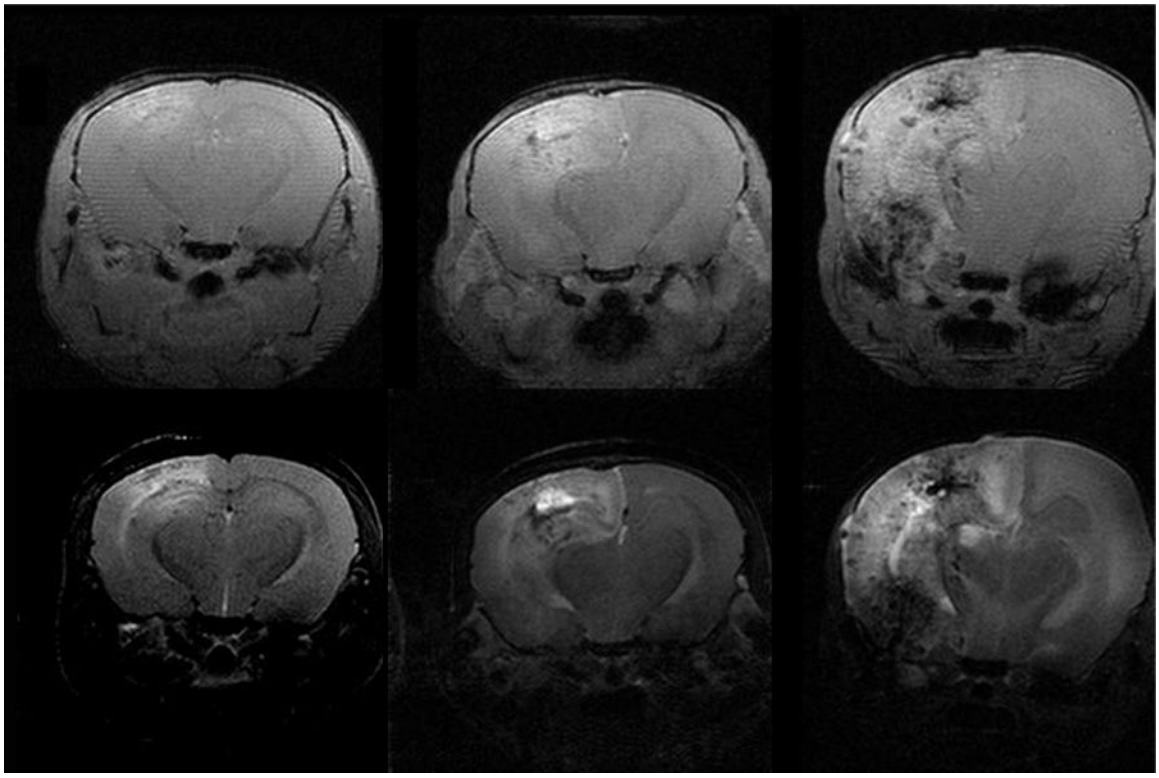

Figure 2.
Representative trans-axial MR images of mice at two (left), three (middle) and four months (right) following fractionated hemispheric irradiation. The upper half of this panel are contrast-enhanced, T1-weighted, gradient-echo images; the lower half of the panel are T2-weighted spin-echo images. Consistent with other animal studies, the left side in each of these images corresponds with the left hemisphere of the mouse's brain, which is the opposite of the convention used when displaying human images. Note the progressive increases in contrast enhancement and T2 signal hyper-intensity with increasing time following irradiation.

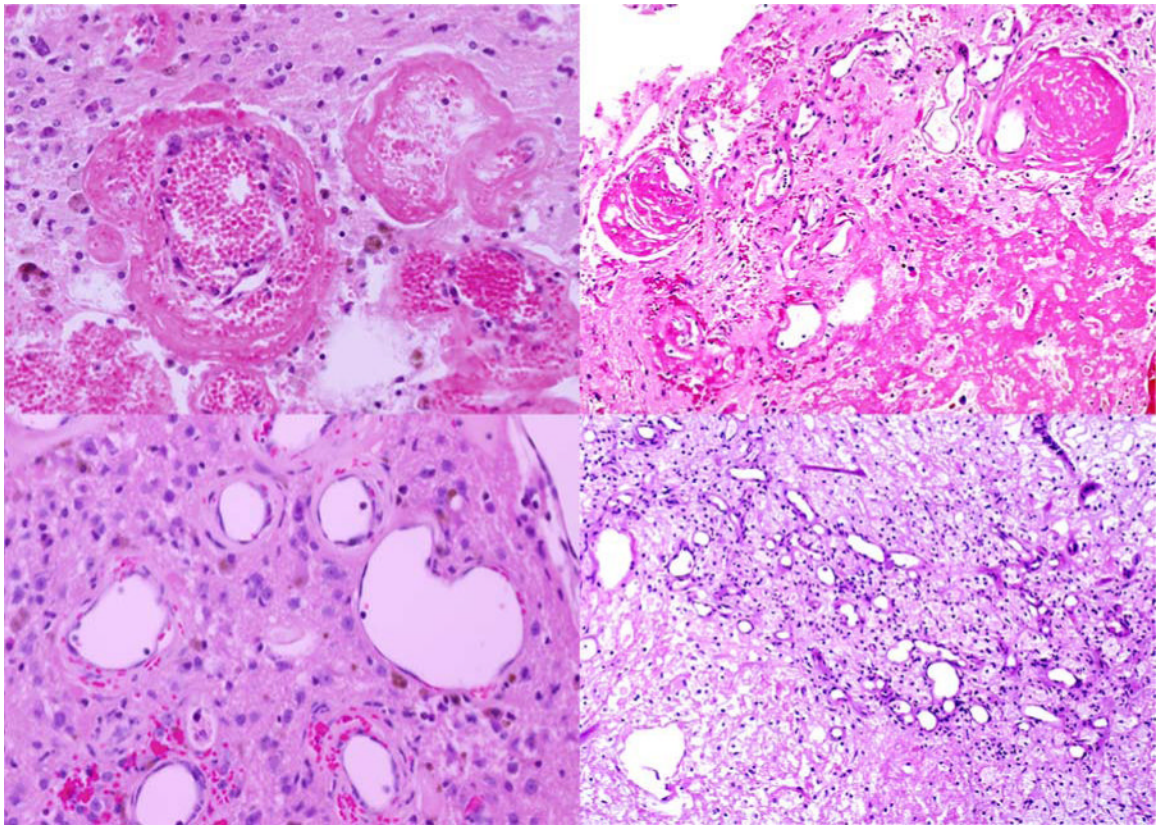

Figure 3.
Representative histological images from (left) a mouse three months after fractionated hemispheric irradiation and (right) a human subject with radiation necrosis. The histology illustrates changes typically observed in radiation necrosis, including (top) fibrinoid vascular necrosis and (bottom) vascular telangiectasia. The similarities between the mouse and human histology are evident by comparing the left and right panels of this figure.

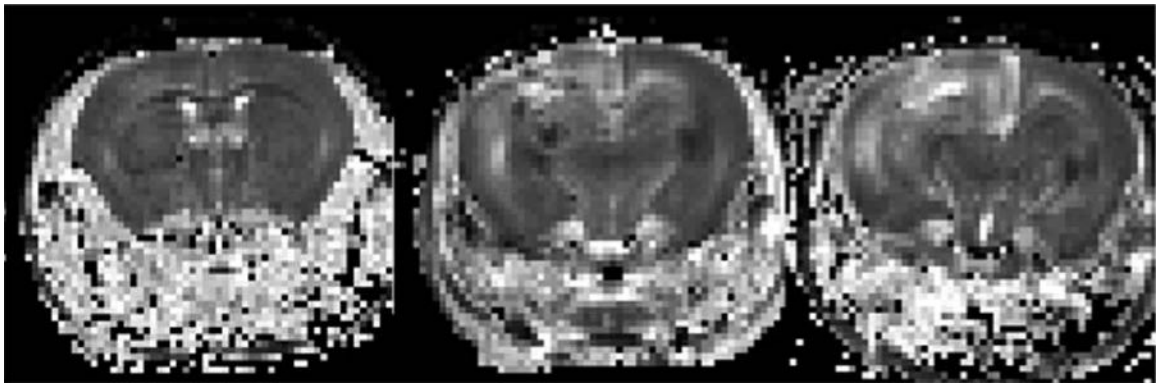

Figure 4.

Apparent diffusion constant (ADC) maps, derived from diffusion-weighted sequences, for animals at two (left), three (center), and four (right) months (from left to right respectively across the panel) following fractionated hemispheric irradiation. The ADC maps correspond precisely with the anatomic images shown in Figure 2. Note the asymmetry in signal intensity and the high diffusivity (characteristically bright signal) in the region of radiation damage corresponding to the anatomic changes seen in Figure 2.

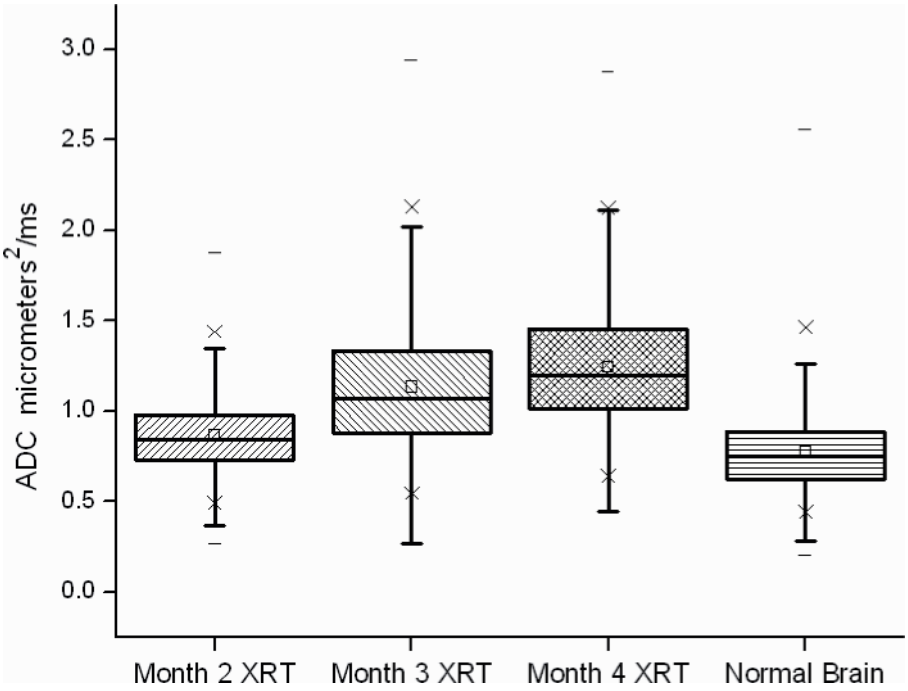

Figure 5.

Box and whisker plot of the ADC values in regions of interest drawn around areas of abnormal signal on b=0 anatomic images and corresponding contralateral untreated brain tissue for all irradiated animals studied. The 25th–75th percentiles are blocked by the box, and the whiskers identify the 99th percentile of the range of diffusivity (ADC) values for each tissue type. A progressive increase in diffusivity is seen that correlates with the progressive tissue damage identified with MR imaging and histology at each time point. There is a statistically significant difference in ADC values between radiated brain tissue and normal brain ($p<0.001$) at each time point.